Role of Pearlitic and Spheroiditic Microstructure in Fatigue Crack Paths

J. Toribio[1], B. González[1] and J. C. Matos[2]

[1] Department of Materials Engineering - University of Salamanca - E.P.S. Zamora (Spain). toribio@usal.es
[2] Department of Computing Engineering - University of Salamanca - E.P.S. Zamora (Spain). jcmatos@usal.es

ABSTRACT. *In this paper the influence of microstructure on fatigue crack growth was analysed in steel with slightly hypereutectoid composition. A material constituted of pearlite colonies and a thin layer of proeutectoid cementite (pearlitic steel) was studied in its initial condition (as received). In addition, the same material was analyzed after undergoing two spheroidization processes consisting of an isothermal treatment on pearlitic steel at 700 ºC and different times (10 and 50 h). Results indicate that fatigue crack propagation curve in the Paris region is not modified by the spheroidization process. Fractometallographic analysis showed a change in the micromechanism of fatigue, evolving from transcollonial (trying to break pearlite lamellae) in the pearlitic steel to intergranular in the spheroidized steel, where cracking takes place through the layer of proeutectoid cementite.*

INTRODUCTION

Spheroidization treatment in pearlite produces fragmentation, spheroidal shape and coalescence in the cementite due to the diffusion processes [1], and these microstructural changes could influence mechanical properties of pearlite. Spheroidization diminishes yield strength, at the same time increasing ductility and fracture resistance [2-4]. In this way, in pearlitic and spheroidized steel, tensile strength depends on the mean slip distance in the ferritic phase, according to the Hall-Petch equation [5-7]. Furthermore, fracture toughness in the pearlitic microstructure increases with the decrease of the prior austenite grain [4], whereas spheroidized steel does so with the increase of the mean free path between cementite carbides [3].

In hypoeutectoid steel, Paris curve [8] does not change with spheroidization, whereas the threshold stress intensity range for fatigue crack propagation in plane strain decreases [9]. Fatigue life under a low number of cycles (strains within the plastic domain) is independent of the carbon contents in the spheroidized steel, while there is a strong dependency with the composition in the pearlitic one [10]. A decrease in the fatigue limit, as well as an increase of the crack growth rate, take place in spheroidized steel with low carbon contents subjected to a small prestrain. However, none of these parameters change

if composition is eutectoid [11]. A slight spheroidization of fine cementite lamellae was observed under tensile fatigue with a high number of cycles, as well as the complete spheroidization of partially spheroidized steel [12]. In pearlitic steel the fatigue surface, formed by ductile micro-tearings, changes its geometry with microstructure and test conditions, and in this case the crack tends to break pearlite lamellae [13]. In the spheroidized microstructure, fatigue fractography presents certain microporosity [12], and the crack is confined in the ferritic matrix except for specimens with high carbon contents tested under high strain ranges, where carbide cracking takes place under fatigue [10].

EXPERIMENTAL PROCEDURE

The material, a slightly hypereuctectoid steel (Table 1), was studied with pearlitic microstructure and after two spheroidization processes obtained by an isothermal treatment on pearlitic steel at 700 ºC, spheroidization times of 10 and 50 h, and cooling inside the furnace (Fig. 1).

Table 1. Chemical composition (wt%) of the steels.

% C	% Mn	% Si	% P	% S	% Al	% Cr	% V
0.789	0.681	0.210	0.010	0.008	0.003	0.218	0.061

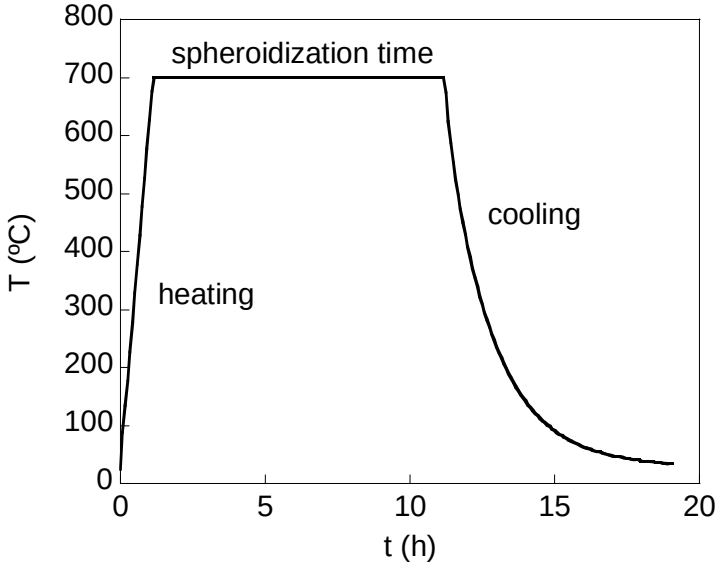

Figure 1. Spheroidization processes (at 700 ºC during 10 h).

The microstructure was observed using a scanning electron microscope (SEM), after small specimens of each material were metalographically prepared (grinding, polishing and etching with 4% Nital). The conventional mechanical properties were obtained using the standard tension test, with a crosshead speed of 2 mm/min.

The fatigue test was performed on bars of 300 mm of length and 11 mm of diameter. Before the test, a small transversal cut was performed on the middle part of the specimens, so as to initiate cracking on this point, and an extensometer (50 mm of length) was placed. The test procedure consisted of applying a sinusoidal oscillating tensile load in the axial direction on decreasing steps, with a constant stress range $\Delta\sigma$ during each step. A 10 Hz frequency was used. The initial maximal stress was lower than the conventional yield strength at 0.2%, decreasing in the next steps around 20÷30% with regards to the maximal stress in the previous step. Every load step was maintained enough time to be able to appreciate the crack advance and eliminate the plastic effect on the crack tip caused by the previous step.

The fatigue fracture surfaces and the longitudinal cuts on the crack specimens (after its metallographic preparation) were observed using the SEM. In all pictures shown, the crack propagation occurred from left to right.

EXPERIMENTAL RESULTS AND DISCUSSION

The relationship between the microstructure and various aspects of the propagation of fatigue cracks in spheroidized steel were analyzed, at both macro and micro levels.

Microstructure

In isothermal treatments of spheroidization there are several factors influencing the spheroidization degree, i.e.: the initial microstructure, the spheroidization temperature, the strain rate (if the material is plastically strained during the treatment) and the time spent inside the furnace [1,14], this being the only variable modified for this research.

Steel without any treatment is made up of pearlite colonies and a thin continuous layer of proeutectoid cementite surrounding the prior austenite grain (Fig. 2). The spheroidization treatment changes the cementite morphology. With a treatment at 700 ºC during 10 h, fragmentation and spheroidization can be observed, but a certain orientation in cementite is maintained and the colony boundaries can still be distinguished (Fig. 3). The increase in the treatment duration (50 h) causes a greater spheroidization and coalescence degree in the cementite, with bigger size particles and a greater distance between them, where the colonies can be barely distinguished (Fig. 4). Therefore, in spheroidized steel, great carbide globules precipitated on the layer of proeutectoid cementite were observed (Figs. 3 and 4), just at locations where the transformation firstly occurs, because its energy is greater than inside the grain [15].

Standard Tension Test

The conventional mechanical properties of steels were obtained by means of standard tension tests from the curves stress σ *vs.* strain ε (Fig. 5). The spheroidization process maintains the Young modulus E nearly constant while at the same time diminishing both the yield strength σ_Y and the ultimate tensile strength (UTS) σ_R, and increasing the strain at maximum load ε_R (Table 2). The fracture surface resulting from the standard tension test for pearlitic steel is mainly made of cleavages (except for the external ring and the zone of central process) which turn into microvoids due to the spheroidization of the steel, with some isolated cleavage.

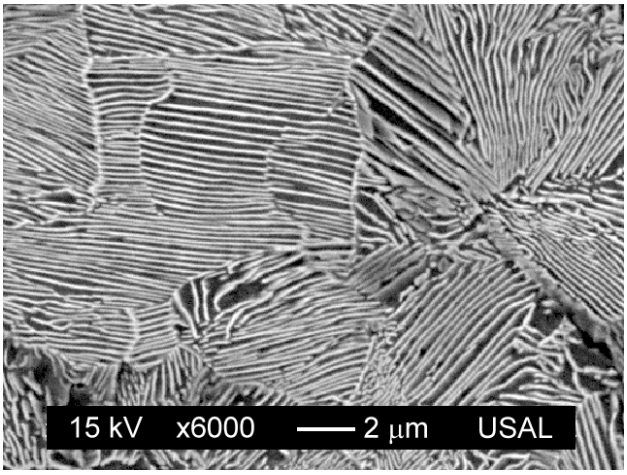

Figure 2. Microstructure of pearlitic steel (slightly hypereutectoid).

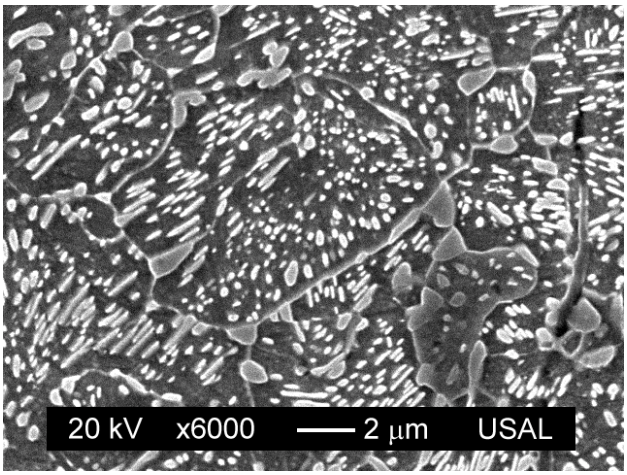

Figure 3. Microstructure of spheroidized steel (at 700 ºC during 10 h).

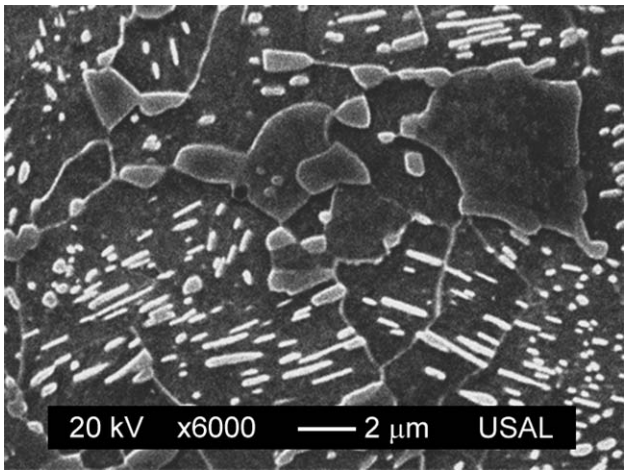

Figure 4. Microstructure of spheroidized steel (at 700 ºC during 50 h).

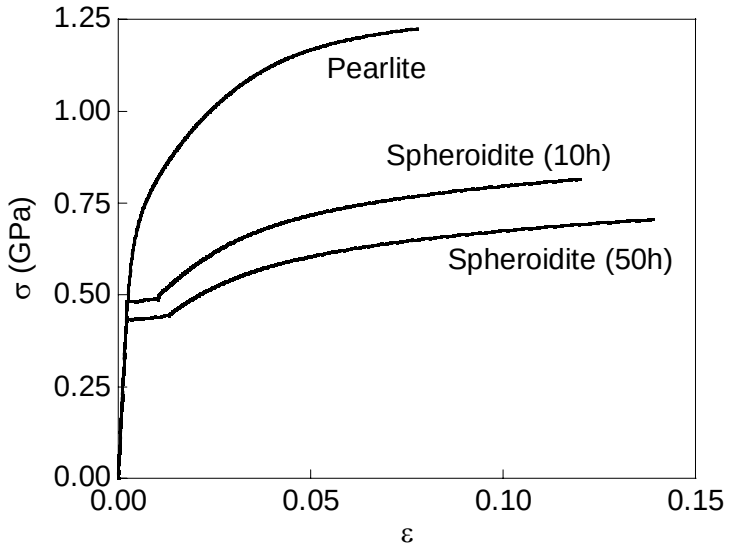

Figure 5. Standard tension tests (σ *vs.* ε).

Table 2. Mechanical properties of pearlitic and spheroidized steels.

Steel	E (GPa)	σ_Y (GPa)	σ_R (GPa)	ε_R
Pearlite	202	0.70	1.22	0.08
Spheroidized at 700 ºC during 10 h	206	0.48	0.82	0.12
Spheroidized at 700 ºC during 50 h	203	0.43	0.70	0.14

Fatigue Crack Propagation

After the tests were carried out, the fatigue crack surfaces of the specimens were photographed (Fig. 6). All steels exhibited mode I fatigue fracture, where the fracture surface was contained in the transversal section of the wire, which is perpendicular to the direction of the load application. In those steels more spheroidized (50 h) a narrow ring of great plasticity can also be observed on the zone close to the surface.

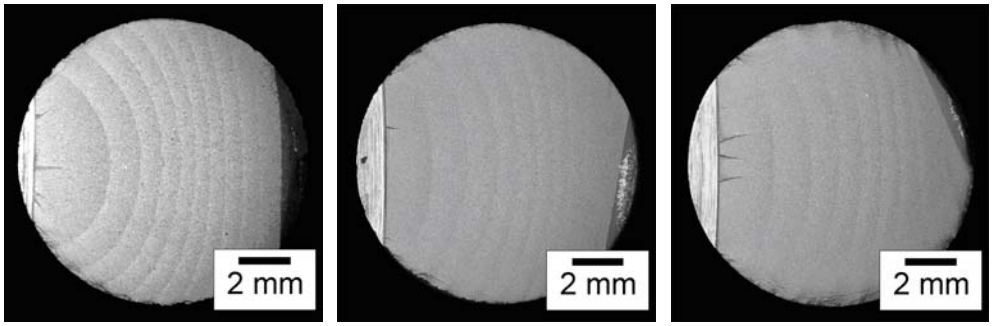

Figure 6. Fatigue fracture surfaces: pearlitic steel, spheroidized steel at 700 ºC during 10 h and spheroidized steel at 700 ºC during 50 h (from left to right).

For every step change on the fatigue surface there can be observed the crack front, which was modelled as part of an ellipse (with centre on the bar surface), with semiaxes *a* (crack depth) and *b* (Fig. 7), from a set of points taken on that front and using the least squares method.

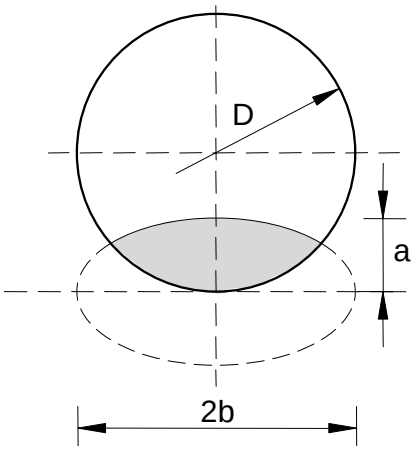

Figure 7. Modelling of the crack front.

At the central point of the crack front (where a plane strain state is reached) the crack growth cyclic rate (d*a*/d*N*) versus the stress intensity factor range (Δ*K*) was calculated. According to the linear elastic fracture mechanics (LEFM), the value of Δ*K* at the crack tip for the geometry studied, crack size *a* and remote axial tensile load is:

$$\Delta K = Y \Delta \sigma \sqrt{\pi a} \tag{1}$$

The dimensionless stress intensity factor (*Y*) was used at the crack centre, calculated by Astiz [16] by using the technique of crack virtual extension and the finite element method. The expression obtained is a function of the following parameters: relative crack depth (crack depth divided by the diameter, *a*/*D*) and the aspect ratio (ratio between the ellipse semiaxes, *a*/*b*), as,

$$Y = \sum_{\substack{i=0 \\ i \neq 1}}^{4} \sum_{j=0}^{3} C_{ij} \left(\frac{a}{D} \right)^{i} \left(\frac{a}{b} \right)^{j} \tag{2}$$

with the C_{ij} coefficients shown in Table 3 [16],

Table 3. Coefficients C_{ij} of Eq. (2), calculated by Astiz [16].

i	*j=0*	*j=1*	*j=2*	*j=3*
0	1.118	-0.171	-0.339	0.130
2	1.405	5.902	-9.057	3.032
3	3.891	-20.370	23.217	-7.555
4	8.328	21.895	-36.992	12.676

The representations 1/*CED versus a*/*D* (where 1/*CED* is the dimensionless stiffness, $C=\Delta u/\Delta F$ being the flexibility obtained from the test registry) and *a*/*b versus a*/*D* were obtained (Figs. 8 and 9). It was observed that 1/*CED* does not change with the treatment, whereas *a*/*b* for short and long cracks of not treated steel presents a greater value compared to those when treated, which is attributed to compressive residual stresses on the wire's surface due to the hot-rolled steel processing. Figure 10 shows the crack propagation curve da/dN-ΔK in the Paris regime (straight line in a double logarithmic plot) in both steels, exhibiting almost no changes with the spheroidization process.

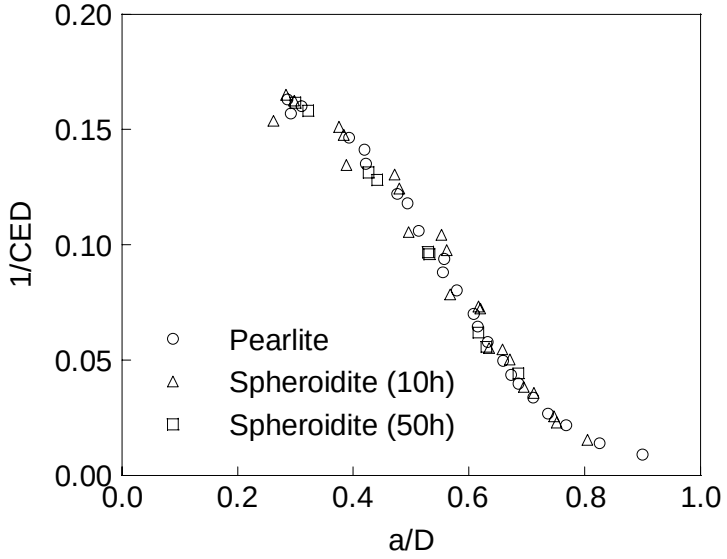

Figure 8. Dimensionless stiffness (1/*CED vs. a*/*D*).

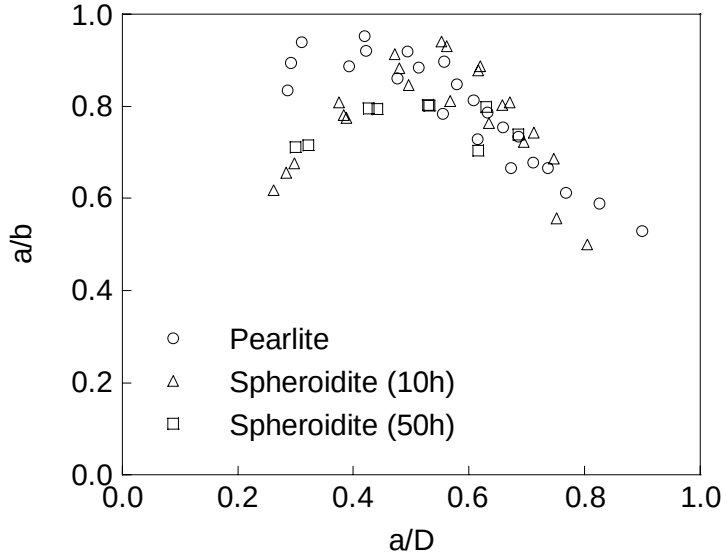

Figure 9. Aspect ratio (*a*/*b vs. a*/*D*).

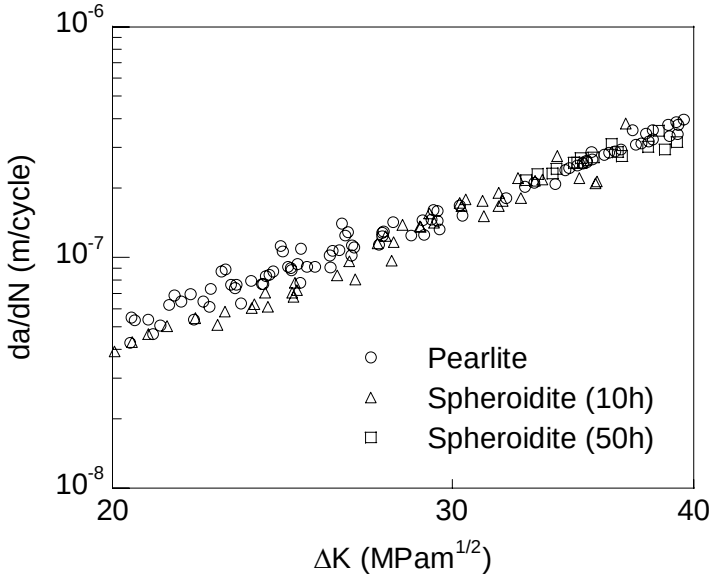

Figure 10. Paris curve (da/dN *vs.* ΔK).

Fractography

Fatigue fractography appearance (Figs. 11 to 13) changes with microstructure (cf. Figs. 2 to 4). In pearlitic steel the fatigue surface is made up of ductile micro-tearings (Fig. 11), where the pearlite lamellae can be seen in some zones (e.g. the central area of the photograph) but it becomes even more ductile (Figs. 12 and 13) with spheroidization, increasing the size of the micro-tearingsand exhibiting bigger voids between them. In addition, the spheroidization treatment produces, to a certain degree, an increase of surface microroughness in the fatigue fractography.

For high values of the maximum stress intensity factor, K_{max}, close to the critical value K_{IC}, fatigue fractography appears mixed with the static mode of the fracture, cleavage as well as small zones of micro-voids for spheroidized steel (which are greater when the treatment is longer).

The fracto-metallographic longitudinal cuts appear on Figs. 14 to 18. The fatigue surface is macroscopically plane in all steels. However, at the microscopic level, the cracking path presents frequent deflections, branches, bifurcations, crack opening changes and discontinuities (Figs. 14 and 15), thereby causing the distinctive geometry of ductile microtearings in the analyzed materials.While the crack in pearlitic steel tends to break the pearlite lamellae causing a transcollonial fracture (Fig. 16), in spheroidized steel the fracture mainly occurs, without breaking globular cementite, through the continuous layer of proeutectoid cementite surrounding the prior austenite grain (Figs. 17 and 18) which is, in this case, the weakest zone of the material in the matter of fatigue.

Therefore, the spheroidization process causes in steel a change in the micromechanisms of fatigue fracture, changing from transcollonial in pearlitic steel (where the key parameters are the size of the pearlitic colony and the pearlite interlamellar spacing), to intergranular (where the parameters driving the fatigue are the size of the prior austenite grain and the layer of proeutectoid cementite surrounding it).

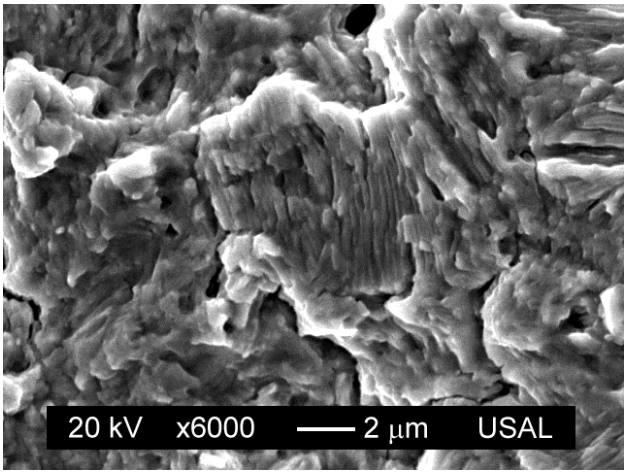

Figure 11. Fatigue fractography in pearlitic steel (slightly hypereutectoid).

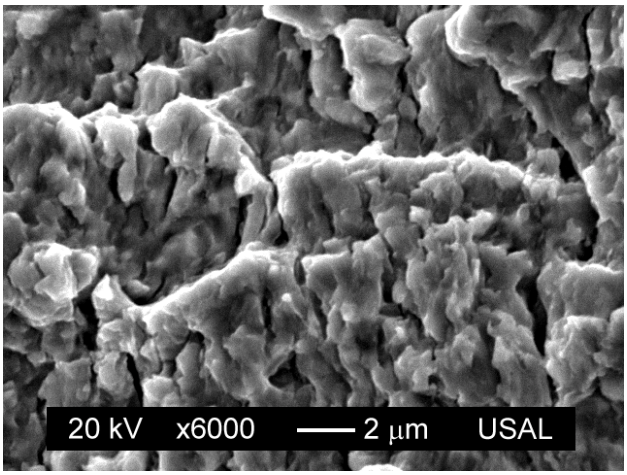

Figure 12. Fatigue fractography in spheroidized steel (at 700 ºC during 10 h).

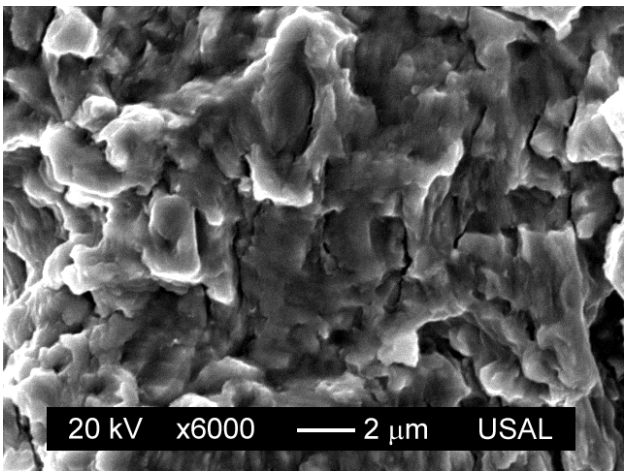

Figure 13. Fatigue fractography in spheroidized steel (at 700 ºC during 50 h).

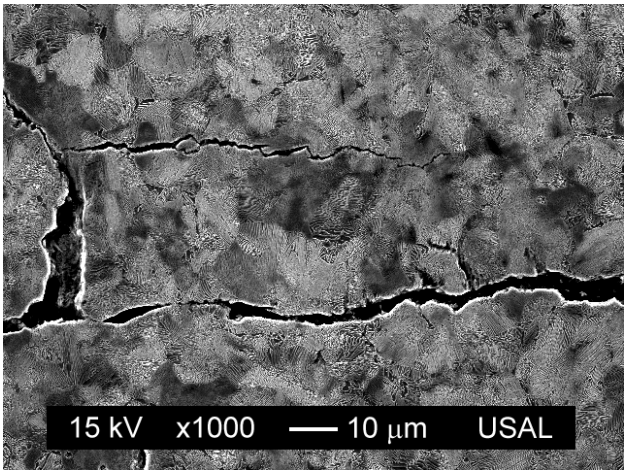

Fig. 14. Fatigue crack in pearlitic steel (slightly hypereutectoid).

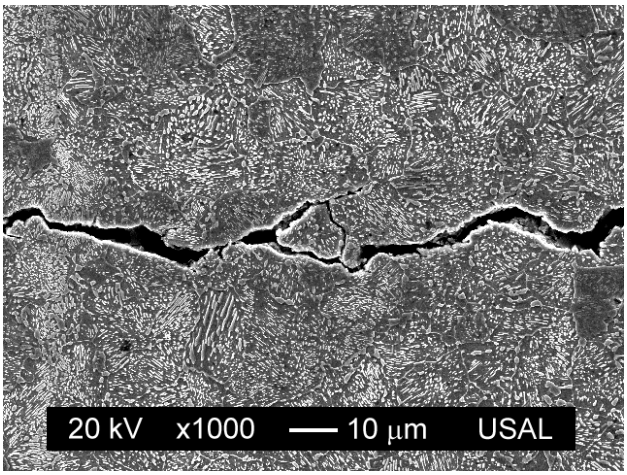

Fig. 15. Fatigue crack in spheroidized steel.

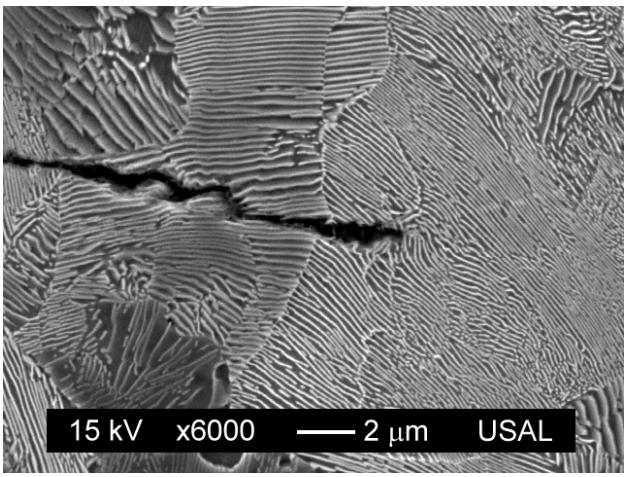

Figure 16. Fatigue micro-crack in pearlitic steel (slightly hypereutectoid).

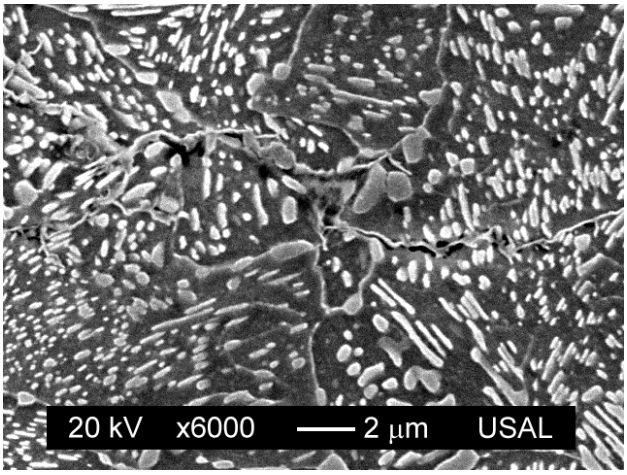

Figure 17. Fatigue micro-crack in spheroidized steel (at 700 ºC during 10 h).

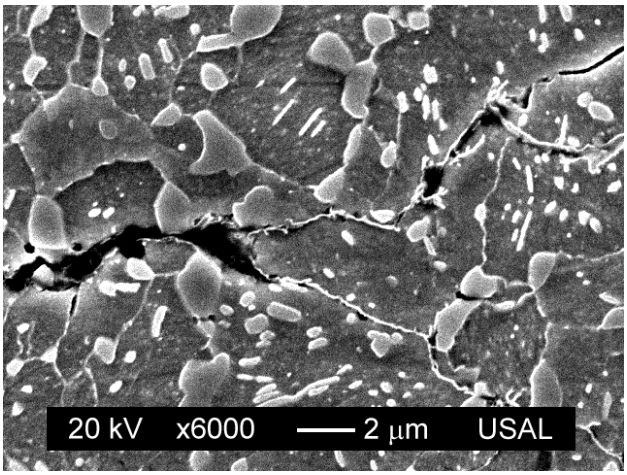

Figure 18. Fatigue micro-crack in spheroidized steel (at 700 ºC during 50 h).

In spite of the changes in the fatigue micromechanisms due to microstructural alterations, the crack propagation curve in the Paris regime (macroscopical aspect of growth) is *not* affected by the spheroidization, because it barely changes with such a heat treatment. However, this treatment decreases the threshold stress intensity factor range ΔK_{th} for fatigue crack growth [9] and increases the fracture toughness K_{IC} [2-4].

CONCLUSIONS

From this research on the influence of pearlite spheroidization on fatigue crack propagation in slightly hypereuctectoid pearlitic steel the following conclusions can be drawn:

(i) The fatigue crack growth curve of pearlitic steel in the Paris regime barely changes after a spheroidization process.

(ii) Macroscopically, the fatigue crack surface in the steel is plane. However, at the microscopic level it shows ductile micro-tearings, the spheroidization producing greater ductile features and bigger voids between them.

(iii) In pearlitic and spheroidized steel the fatigue crack presents at microscopical level a propagation path with frequent deflections, branches, bifurcations, changes on the crack opening and discontinuities.

(iv) The micromechanism of fatigue fracture changes with the spheroidization. Microcracking in pearlitic steel tends to break the pearlite lamellae, whereas in spheroidized steel it occurs through the thin layer of proeutectoid cementite surrounding the prior austenite grain, without fracturing the particles of globular cementite in the main areas of the material.

ACKNOWLEDGEMENTS

The authors wish to acknowledge the financial support provided by the following Spanish Institutions: Ministry for Science and Technology (MCYT; Grant MAT2002-01831), Ministry for Education and Science (MEC; Grant BIA2005-08965), Ministry for Science and Innovation (MICINN; Grant BIA2008-06810 and BIA2011-27870), Junta de Castilla y León (JCyL; Grants SA067A05, SA111A07 and SA039A08), and Fundación Samuel Solórzano Barruso (Grant FS/16-2010).

REFERENCES

1. Chattopadhyay, S., Sellars, C.M. (1982) *Acta Metall.* **30(1)**, 157-170.
2. Rosenfield, A., Hahn, G., Embury, J. (1972) *Metall. Trans.* **3(11)**, 2797-2804.
3. Firrao, D., Anzalone, S.A., Begley, J.A. (1984) *Metall. Sci. Tech.* **2(1)**, 15-23.
4. Fernández-Vicente, A., Carsí, M., Peñalba, F., Taleff, E., Ruano, O.A. (2002) *Mater. Sci. Eng.* ***A*****335(1-2)**, 175-185.
5. Hall, E.O. (1951) *Proc. Phys. Soc. London Sect.* ***B*****64(9)**, 747-753.
6. Petch, N.J. (1953) *J. Iron Steel Inst.* **174**, 25-28.
7. Karlsson, B., Lindén, G. (1975) *Mater. Sci. Eng.* **17(1)**, 153-164.
8. Paris, P.C., Erdogan, F. (1963) *J. Basic Eng.* **85D**, 528-534.
9. Kim, E.S., Kim, I.S. (2000) *J. Mater. Sci. Lett.* **19(5)**, 367-369.
10. Milligan, R. (1974) *Exp. Mech.* **14(5)**, 190-195.
11. Nagase, Y., Kanri, T. (1992) *Fatigue Fract. Eng. Mater. Struct.* **15(2)**, 213-223.
12. Savrai, R., Makarov, A., Schastlivtsev, V., Tabatchikova, T., Yakovleva, I., Egorova, L. (2010) *Russ. Metall.+ (Metally)* **2010(4)**, 310-315.
13. Toribio, J., Matos, J.C., González, B. (2009) *Int. J. Fatigue* **31(11-12)**, 2014-2021.
14. Kamyabi-Gol, A., Sheikh-Amiri, M. (2010) *J. Iron Steel Res. Int.* **17(4)**, 45-52.
15. Zhang, S.L., Sun, X.J., Dong, H. (2006) *Mater. Sci. Eng.* ***A*****432(1-2)**, 324-332.
16. Astiz, M.A. (1986) *Int. J. Fract.* **31(2)**, 105-124.